Journal of Southeast University (English Edition) Vol. 36, No. 1, pp. 24 - 31 Mar. 2020 ISSN 1003—7985

Stability analysis of the rotating tribological pair system on circular-disc end faces

Chen Long Zhang Jianrun

(School of Mechanical Engineering, Southeast University, Nanjing 211189, China)

Abstract: In order to study the stability of friction and contact of the rotating tribological pair system, considering the influence of the changeable factors on the stability, the system dynamics analysis model based on the Lagrange equation is firstly established. The surface contact stiffness model is determined on the basis of the fractal theory. The model of the friction torque with velocities is created by using the Stribeck friction effect. The Lyapunov indirect method is employed to explore the eigenvalue problem of the system state equation. The effects of the applied load, the fractal dimension, the fractal scaling coefficient and the Stribeck coefficient on the system stability are investigated in detail. The numerical simulation results demonstrate that the tribological pair system is prone to causing system instability at low speed, and the system instability boundary value decreases when the Stribeck coefficient decreases. The fractal dimension and the fractal scaling coefficient impact the system stability slightly when fractal dimensions are large, and the system instability can be reduced by properly increasing the surface smoothness. Moreover, the system instability evidently increases with the increase in the applied load and the Stribeck coefficient. These achievements can provide a reference and theoretical support for the analysis of the dynamic performance of the tribological pair system.

Key words: rotating tribological pair system; contact stiffness; Stribeck effect; dynamic model; stability

DOI: 10.3969/j.issn.1003 - 7985.2020.01.004

High-speed rotating structures form friction in the end, which results in an unstable operation of the system and brings frictional vibration and noise. This is a common phenomenon in engineering, for instance, brakes, clutches, compressors' crankshafts and the train wheel-rail. The mechanical model of this end rotating friction structure is a pair of high-speed disc tribological pairs. Several physical mechanisms that attempt to explain unstable friction-induced vibration have been proposed in the literature and were reviewed in Ref. [1]: the negative friction slope[2], sprag-slip instability[3], stick-slip instability[4], and mode-coupling instability[5]. However, there has been no universal consensus of an explanation for friction phenomena and the dynamic behavior of friction-induced vibration is not fully understood.

For reducing the impact of friction on engineering and the environment, many studies have been carried out with analytical, computational and experimental techniques. To explore the frictional system, the early achievements are attributed to the dry frictional stick-slip self-excited vibration[6] and unstable structural vibration[7]. Stick-slip is often caused by the nonlinear stiffness effect[8] or nonlinear discontinuity in μ-v friction curve[9]. Hereby, the Stribeck coefficient is usually included in the stick-slip analysis to analyze the system stability and determine the critical speed of the dynamic model[10-11]. Whereas, stick-slip theory ignores the interaction between two contacting surfaces. To overcome this shortcoming, elastic or flexible discs have been adopted. Ouyang et al.[12] examined the transverse instability of an elastic disc under the action of a rotating friction slider with stick-slip vibration. Ouyang and Mottershead[13] investigated the instability of the transverse vibration of a disk excited by two co-rotating sliders on either side of it, taking into account the bending couple acting in the circumferential direction produced by the different friction forces on the two sides of the disk. Studies show that the modal coupling theory can explain most friction phenomena under different friction causes. Hoffmann and Gaul[5] studied the qualitative and quantitative aspects of the mode-coupling instability with the presence of structural damping in sliding friction systems. Kang[14] analyzed the dynamic instability induced by friction in the ball joint system and presented the conditions of the mode-coupling instability. Sui and Ding[15] established a pad-on-disc frictional model and carried out the eigenvalue analysis to evaluate the stability of the pad considering the stochastic variation of frictional coefficients and the contact effect.

The features of contact at the friction interface of the disc are ignored in most of the studies mentioned above. Actually, the contact stiffness is inevitably affected by the tribological pairs under the contact condition, causing the variety in system instability. For establishing an accurate

Received 2019-11-02, **Revised** 2020-01-03.

Biographies: Chen Long (1994—), male, graduate; Zhang Jianrun (corresponding author), male, doctor, professor, zhangjr@seu.edu.cn.

Foundation items: The Science and Technology Support Program of Jiangsu Province (No. BE2014133), the Transformation Program of Scientific and Technological Achievements of Jiangsu Province (No. 201701213).

Citation: Chen Long, Zhang Jianrun. Stability analysis of the rotating tribological pair system on circular-disc end faces[J]. Journal of Southeast University (English Edition), 2020, 36(1): 24 - 31. DOI: 10.3969/j.issn.1003 - 7985.2020.01.004.

dynamic analysis model, the contact stiffness model should be proposed in addition. As the fractal model can simulate the contact state with high precision, researchers have developed some fractal contact stiffness models and explored the influence of vital parameters on the model such as the fractal dimension D, the fractal scaling coefficient G and the applied load[16–19]. Due to the effects of friction, some scholars put forward some modified models to correct the contact stiffness[20–21]. It can be concluded that the contact stiffness is modifiable with various system characteristic parameters.

Therefore, a dynamic analysis model of the rotating tribological pair system on the circular-disc end face for determining the system stability is proposed according to the Stribeck effect and fractal contact characteristics in this paper. The dynamic differential equation of the system is modeled by the Lagrange equation. The friction torque considering the Stribeck effect is produced, and the normal contact stiffness and the tangential contact stiffness are established through the fractal theorem. The system equation is deduced and the criterion of system stability is given. The system stability is investigated and discussed by the numerical simulation analysis of the effects of applied loads, Stribeck coefficients, and fractal parameters D and G. The achievements of this work will serve as a reference and a theoretical support for the analysis of the dynamic performance of frictional systems.

1 Dynamic Model of Rotating Tribological Pair System on the End Face

The instability of the friction pair is the cause of the instability of the system. Studying the rotational freedom and axial freedom of the friction pair can accurately describe the motion state of the friction pair. The dynamic model of a non-damping system is established, as shown in Fig. 1. m_1 and J_1 represent the mass and torque of inertia of the active part, respectively; m_2 and J_2 represent the mass and torque of inertia of the driven part; both of them are metal parts. The displacement x_1 is along the X direction; θ_1 and θ_2 are the rotation angles of the active and driven parts. The driven part connecting to the base is subject to the elastic constraints of k_1 and k_2; k_1 is in the X direction and k_2 is in the direction of the circumference tangent. The parameter k_n is the normal contact stiffness and k_t represents the tangential contact stiffness, and they are used to connect the active part and the driven part. The load p is applied along the X direction; M_0 is the driving torque of the active part. r_1 and r_2 are the radii of the inner and outer rings of the pair on the contact surface, as shown in Fig. 1(b). We assume that point B and point B' are in the same position; point B is on the surface of the active part, but point B' is on the driven part; there is a spring connecting two points in the circumference tangential direction, so k_t is the total tangential contact

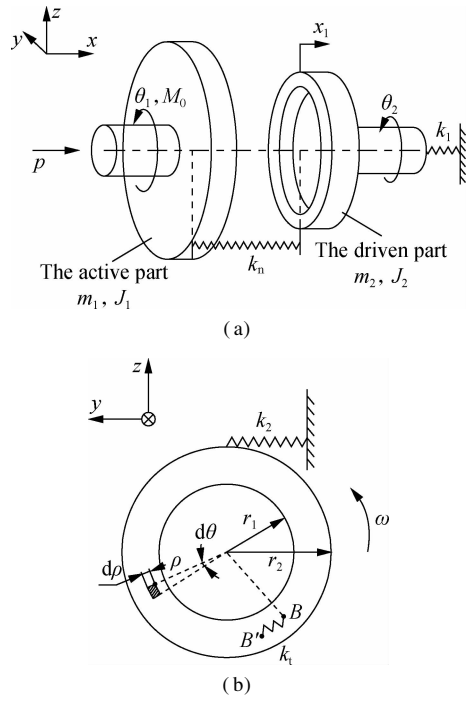

Fig. 1 The rotating tribological pair system on the circular-disc end face. (a) Diagram of friction pair system; (b) The contact surface

stiffness on the contact surface.

In a system dynamics analysis, it is worth considering whether the flexibility of components affects the dynamic calculations. Generally speaking, the natural frequencies of the metal components being studied in this paper are much higher, and their thicknesses are not thin, so the flexibility of the component can be ignored. With the Lagrange system modeling method, the general form of the Lagrange second-class equation can be described as

$$\frac{\mathrm{d}}{\mathrm{d}t}\left(\frac{\partial T}{\partial \dot{q}_i}\right)-\frac{\partial T}{\partial q_i}+\frac{\partial V}{\partial q_i}=Q_i^* \tag{1}$$

where T is the kinetic energy of the system; V is the potential energy of the system; q_i is the generalized coordinate of the system; $\dot{q}_i$ is the generalized velocity of the system; Q_i^* is the generalized force of the system.

Then, we have the dynamic differential equation of the system,

$$\begin{bmatrix} J_1 & & \\ & J_2 & \\ & & m_2 \end{bmatrix}\begin{bmatrix} \ddot{\theta}_1 \\ \ddot{\theta}_2 \\ \ddot{x}_1 \end{bmatrix}+ \begin{bmatrix} k_t r_2^2 & -k_t r_2^2 & 0 \\ -k_t r_2^2 & (k_t+k_2) r_2^2 & 0 \\ 0 & 0 & k_n+k_1 \end{bmatrix}\begin{bmatrix} \theta_1 \\ \theta_2 \\ x_1 \end{bmatrix}=\begin{bmatrix} M_0-M_f \\ M_f \\ p \end{bmatrix} \tag{2}$$

Consequently, the dynamic model of the rotating tribological pair system on the end face is set up, and it is a basic equation for exploring the system stability. The friction, a cause of system instability, can generate a negative damping in systems. Among the studies mentioned above, most of them modeled the friction force in the ro-

tating system, which cannot describe the frictional features of the complete contact surfaces precisely; thus, the friction torque M_f taking into account the Stribeck effect is adopted in this paper. Under the consideration of the contact stiffness, the values of k_n and k_t are often given definitely, omitting the contact characteristics and the effect of friction. However, the contact state is also a significant factor of the system stability, which can alter the systemic stable state, so the contact stiffness should be established correctly. The specific modeling progresses are given in the following sections.

2 Friction and Contact Mathematical Model

2.1 Stribeck friction torque model

When the friction phenomenon is described by differential equations, the friction models are roughly divided into two categories: the static friction model and the dynamic friction model[22]. Armstrong-Hélouvry and Soom[23] suggested that a good static friction model could approximate the actual friction with 90% accuracy. For mathematically representing the Stribeck phenomenon, an extensively used model describing the Stribeck effect, the Gauss index model, is employed, in which the Stribeck friction coefficient dependent on the relative velocity is approximated by the following function:

$$f_s(v) = \mu_k + (\mu_s - \mu_k)\, e^{(-v/v_s)^2} \tag{3}$$

where $f_s(v)$ is the Stribeck friction coefficient; μ_k is the sliding friction coefficient; μ_s is the maximum static friction coefficient; v_s is the Stribeck coefficient.

Then, the first derivative of $f_s(v)$ is

$$f_s'(v) = -\frac{2v}{v_s^2}(\mu_s - \mu_k)\, e^{(-v/v_s)^2} \tag{4}$$

Fig. 2 exhibits the friction coefficient curves at different Stribeck coefficients with $\mu_s = 0.18$ and $\mu_k = 0.12$, which evidently illustrate the negative slope of friction-velocity. Therefore, the Stribeck coefficient should be deliberated in order to evaluate friction accurately.

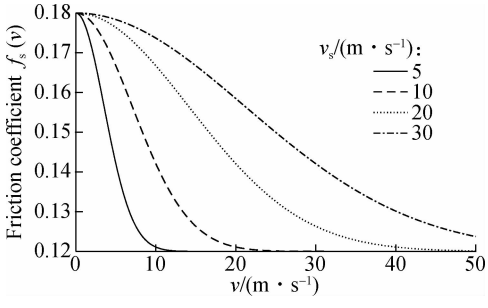

Fig. 2 Stribeck friction coefficient curves

The friction force is modeled considering the Stribeck effect in most studies, while the friction torque is more suitable for presenting the rotating tribological pair system. Before modeling the friction torque, the micro-element surface on the contact surface is taken into account, as shown in Fig. 1(b). At the radius ρ, the area of the micro-element is

$$dS = \rho d\theta d\rho \tag{5}$$

From Fig. 1(a), we have the total contact load $p_n = k_n x_1$. Assuming that the contact load is uniformly distributed on the surface, the load on the micro-element is

$$dp = \frac{p_n}{A_a} dS = \frac{k_n x_1}{A_a} \rho d\theta d\rho \tag{6}$$

where A_a is the nominal contact area; k_n is the normal contact stiffness; x_1 is the displacement of the contact surface.

In order to describe the Stribeck effect on the friction, we introduce the Stribeck friction coefficient $f_s(v)$ into the friction torque. The moment of friction force applied on the micro-element surface to the rotation axis is founded as

$$dM_f = \rho f_s(v)\, dp = \frac{k_n x_1}{A_a} f_s(\omega\rho) \rho^2 d\theta d\rho \tag{7}$$

where ω is the relative rotation angular velocity, $v = \omega\rho$.

According to Eq. (7), the moment has the same expression at any angles, and then we can obtain the friction torque M_f of the entire contact surface,

$$M_f = \int_0^{2\pi} \int_{r_1}^{r_2} dM_f = \frac{2\pi k_n x_1}{A_a} \int_{r_1}^{r_2} f_s(\omega\rho) \rho^2 d\rho \tag{8}$$

where r_1 and r_2 are the radii of the inner and outer rings of the contact surface.

2.2 Contact stiffness fractal model

The development of the fractal theory has greatly promoted the study of surface microscopic features, which makes the contact characteristic parameters closer to the actual situation. The accurate description of the contact state is an essential prerequisite for modeling. Therefore, the establishment of k_n and k_t is described in the following.

The contact problem between two rough surfaces is generally equivalent to the contact problem between a rough surface and an ideal plane. Therefore, Young's modulus E of the equivalent rough surface is given by

$$\frac{1}{E} = \frac{1 - \nu_1^2}{E_1} + \frac{1 - \nu_2^2}{E_2} \tag{9}$$

where E_1, E_2, ν_1 and ν_2 are the two materials' Young's modulus and Poisson's ratios.

The relationship between the total dimensionless contact load p^* and the dimensionless real contact area A_r^* of the rough surface is provided by the M-B fractal contact model[24] under the elastic-plastic contact condition.

If $1 < D < 2$ and $D \neq 1.5$, the dimensionless contact load p^* is expressed as

$$p^* = \frac{4\sqrt{\pi}}{3}G^{*(D-1)}g_1(D)A_r^{*(D/2)}\left[\left(\frac{2-D}{D}A_r^*\right)^{(3-2D)/2} - a_c^{*(3-2D)/2}\right] + K\phi g_2(D)A_r^{*(D/2)}a_c^{*(2-D)/2} \tag{10}$$

If $D=1.5$, the expression of p^* is written as

$$p^* = \sqrt{\pi}G^{*1/2}\left(\frac{A_r^*}{3}\right)^{3/4}\ln\left(\frac{A_r^*}{3a_c^*}\right) + 3K\phi\left(\frac{A_r^*}{3}\right)^{3/4}(a_c^{*1/4}) \tag{11}$$

where D is the fractal dimension; G is the fractal scaling coefficient. D and G can be obtained by the parameter identification of the surface. a_c is the critical micro-contact area at the boundary point of the elastic-plastic deformation, which is described as

$$a_c = G^2\left(\frac{K\phi}{2}\right)^{2/(1-D)} \tag{12}$$

where $K = H/\sigma_s$; $\phi = \sigma_s/E$; H and σ_s are the hardness and yield strength of the softer material. $g_1(D)$ and $g_2(D)$ are constants of the fractal dimension, which can be calculated as

$$\left.\begin{aligned} g_1(D) &= \frac{D}{3-2D}\left(\frac{2-D}{D}\right)^{D/2} \\ g_2(D) &= \left(\frac{D}{2-D}\right)^{(2-D)/2} \end{aligned}\right\} \tag{13}$$

The dimensionless parameters are defined as

$$p^* = \frac{p}{A_a E},\quad G^* = \frac{G}{\sqrt{A_a}},\quad A_r^* = \frac{A_r}{A_a},\quad a_c^* = \frac{a_c}{A_a} \tag{14}$$

where A_a is the nominal contact area; A_r is the real contact area; p is the applied load.

Referring to Ref. [21] and considering the influence of friction, the critical micro-contact area is revised as

$$a_c = G^2\left(\frac{3.3\sqrt{\pi}k_\mu\phi}{4}\right)^{2/(1-D)} \tag{15}$$

where k_μ is a friction correction factor, and its expression depending on the friction coefficient μ is

$$k_\mu = \begin{cases} 1-0.228\mu & 0\leqslant\mu\leqslant 0.3 \\ 0.932\mathrm{e}^{-1.58(\mu-0.3)} & 0.3<\mu\leqslant 0.9 \end{cases} \tag{16}$$

Approximately regarding the micro-convex body as a sphere, the normal contact stiffness $\mathrm{d}k_n$ depending on the contact area a of one single micro-convex body is described as

$$\mathrm{d}k_n = \frac{4}{3\sqrt{\pi}}Ea^{1/2} \tag{17}$$

The maximum contact area a_1 has the following relationship with the real contact area A_r,

$$a_1 = \frac{2-D}{D}A_r \tag{18}$$

Thus, the total normal contact stiffness k_n of the rough surface is determined as

$$k_n = \frac{4ED}{3\sqrt{\pi}(1-D)}\left(\frac{2-D}{D}A_r\right)^{D/2}\cdot\left[\left(\frac{2-D}{D}A_r\right)^{(1-D)/2} - a_c^{(1-D)/2}\right] \tag{19}$$

According to Ref. [17], the tangential contact stiffness k_t can be modeled as

$$k_t = \frac{4ED}{\sqrt{\pi}(1+\nu)(2-\nu)(1-D)}\left(1-\frac{1}{\mu}\frac{T_0}{p}\right)^{1/3}\cdot\left(\frac{2-D}{D}A_r\right)^{D/2}\left[\left(\frac{2-D}{D}A_r\right)^{(1-D)/2} - a_c^{(1-D)/2}\right] \tag{20}$$

where T_0 is the tangential load.

3 System Equation Deduction for the Stability Criterion

For determining the system stability, the friction torque M_f should be linearized due to the nonlinear Stribeck coefficient $f_s(v)$. According to Eq. (8), the Taylor expansion at $x_1 = x_{10}$, $\omega = \omega_1$ is written as

$$M_f = x_1\frac{2\pi k_n}{A_a}\int_{r_1}^{r_2} f_s(\omega_1\rho)\rho^2\mathrm{d}\rho - \frac{2\pi k_n x_{10}(\omega-\omega_1)}{A_a}\int_{r_1}^{r_2} f_s'(\omega_1\rho)\rho^3\mathrm{d}\rho \tag{21}$$

where $x_{10} = p/k_n$; $\omega_1 = \dot\theta_1 = v_t/\rho$; and v_t is the linear velocity at the radius ρ.

Then, the friction torque can be expressed as

$$M_f = h_1x_1 - h_2\dot\theta_2 \tag{22}$$

where the definitions of h_1 and h_2 are given by

$$\left.\begin{aligned} h_1 &= \frac{2\pi k_n}{A_a}\int_{r_1}^{r_2} f_s(v_t)\rho^2\mathrm{d}\rho \\ h_2 &= \frac{2\pi p}{A_a}\int_{r_1}^{r_2} f'(v_t)\rho^3\mathrm{d}\rho \end{aligned}\right\} \tag{23}$$

Hence, the dynamic equation of the tribological pair system can be constructed as

$$\begin{bmatrix} J_1 & & \\ & J_2 & \\ & & m_2 \end{bmatrix}\begin{bmatrix} \ddot\theta_1 \\ \ddot\theta_2 \\ \ddot x_1 \end{bmatrix} + \begin{bmatrix} 0 & -h_2 & 0 \\ 0 & h_2 & 0 \\ 0 & 0 & 0 \end{bmatrix}\begin{bmatrix} \dot\theta_1 \\ \dot\theta_2 \\ \dot x_1 \end{bmatrix} + \begin{bmatrix} k_t r_2^2 & -k_t r_2^2 & h_1 \\ -k_t r_2^2 & (k_t+k_2)r_2^2 & -h_1 \\ 0 & 0 & k_n+k_1 \end{bmatrix}\begin{bmatrix} \theta_1 \\ \theta_2 \\ x_1 \end{bmatrix} = \begin{bmatrix} M_0 \\ 0 \\ p \end{bmatrix} \tag{24}$$

With the deliberation of the Lyapunov indirect method[25], Eq. (24) is rewritten in the state vector form:

$$\begin{bmatrix} \dot\theta_1 \\ \dot\theta_2 \\ \dot x_1 \\ \dot y_1 \\ \dot y_2 \\ \dot y_3 \end{bmatrix} = \begin{bmatrix} y_1 \\ y_2 \\ y_3 \\ \frac{1}{J_1}[M_0 + h_2y_2 - k_t r_2^2(\theta_1-\theta_2) - h_1x_1] \\ \frac{1}{J_2}[-h_2y_2 + k_t r_2^2\theta_1 - (k_t+k_2)r_2^2\theta_2 + h_1x_1] \\ \frac{1}{m_2}[p - (k_n+k_1)x_1] \end{bmatrix} \tag{25}$$

Then, the coefficient matrix $\boldsymbol{A}$ of the system can be determined from Eq. (25):

$$\boldsymbol{A}=\begin{bmatrix}\boldsymbol{O}_{3\times3} & \boldsymbol{I}_{3\times3}\\ \boldsymbol{A}_1 & \boldsymbol{A}_2\end{bmatrix} \tag{26}$$

where $\boldsymbol{O}_{3\times3}$ is the null matrix; $\boldsymbol{I}_{3\times3}$ is the unit matrix; $\boldsymbol{A}_1$ and $\boldsymbol{A}_2$ are defined as

$$\boldsymbol{A}_1=\begin{bmatrix}-\dfrac{k_t r_2^2}{J_1} & \dfrac{k_t r_2^2}{J_1} & -\dfrac{h_1}{J_1}\\ \dfrac{k_t r_2^2}{J_2} & -\dfrac{k_t+k_2}{J_2}r_2^2 & \dfrac{h_1}{J_2}\\ 0 & 0 & -\dfrac{k_n+k_1}{m_2}\end{bmatrix}$$

$$\boldsymbol{A}_2=\begin{bmatrix}0 & \dfrac{h_2}{J_1} & 0\\ 0 & -\dfrac{h_2}{J_2} & 0\\ 0 & 0 & 0\end{bmatrix}$$

Therefore, all the parameters modeled above are substituted into Eq. (26) for computing the eigenvalues of the matrix $\boldsymbol{A}$ through MATLAB. In the light of the stability determination theorem, the eigenvalues λ of the coefficient matrix $\boldsymbol{A}$ have negative real parts on the basis of one approximation, which strongly indicates that the original nonlinear system is asymptotically stable at the equilibrium point. On the other hand, the positive real part of the eigenvalue implies the instability of the system.

4 Numerical Results and Discussion

In this paper, the stability analysis of the rotating tribological pair system on the end face is carried out with the dynamic model. The example of calculating the eigenvalues of matrix $\boldsymbol{A}$ is studied in this section with the given parameter values shown in Tab. 1.

Tab. 1 Model calculation parameters

Parameter	Value	Parameter	Value
p/N	5 000	E_2/GPa	210
k_1/(MN · m^{-1})	10	ν_1	0.27
k_2/(GN · m^{-1})	10	ν_2	0.3
r_1/m	0.03	σ_s/MPa	250
r_2/m	0.06	H/HB	209
m_1/kg	27.2	v_s/(m · s^{-1})	10
m_2/kg	16.7	μ_s	0.18
J_1/(kg · m^2)	480	μ_k	0.12
J_2/(kg · m^2)	320	D	1.80
E_1/GPa	190	G/nm	3.6

The curves of the real part of eigenvalues Re(λ) at different speeds demonstrate that the system tends to be stable at higher speed whereas the system exhibits an unstable state at lower speed, as shown in Fig. 3. Moreover, the real part of the first-order eigenvalue is invariably equivalent to zero, and the third-order shows a positive real part inferring system instability. Hence, the second- and third- order eigenvalues become the focus of this study. Due to the friction characteristics, there are many factors influencing the system stability such as the surface roughness R_a, the applied load p and the Stribeck coefficient v_s, and their effects on the system stability are explored and compared as follows.

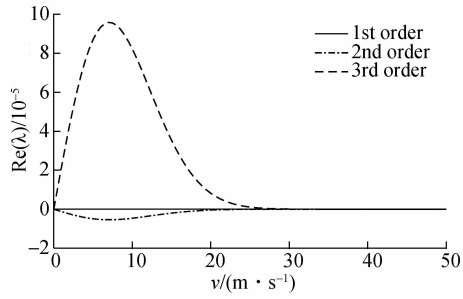

Fig. 3 Real part of eigenvalue

The topography of the surface is one of the important factors affecting the state of frictional contact between surfaces. Statistical methods describe surface features through statistical parameters such as the surface roughness R_a, but the fractal theory uses fractal parameters to solve the problem of scale correlation. The surface roughness and fractal parameters are used as surface characteristics, so scholars have studied the relationship between them. Guan et al. [26] pointed out that the fractal dimensions of processed surfaces with the same manufacturing method are basically equal, and the fractal scaling coefficient changes with surface roughness. Pan et al. [27] analyzed the relationship between surface roughness and fractal parameters in details. When the fractal scaling coefficient G is small, the surface roughness R_a and the fractal dimension D have a monotonically decreasing relationship; when D value remains unchanged, the relationship between R_a and G can be expressed as

$$R_a \propto G^{D-1} \tag{27}$$

Therefore, the effect of surface roughness on the analysis model is indirectly reflected by studying the fractal parameters.

Fig. 4 describes the variation of the real part of the second-order and third-order eigenvalues of the system with four fractal dimensions. It can be inferred from Fig. 4(b) that the fractal dimension has little impact on the system instability, but its value at 1.75 makes the system unstable with the lowest trend. The relationship between the speed and the real part of eigenvalues at four different fractal scaling coefficients is shown in Fig. 5. It obviously appears that the instability trend of the system increases first and then decreases along with the increase in the fractal scaling coefficient. Actually, when the fractal dimension D increases and the fractal scaling coefficient G decreases, the surface is smoother. The appropriate in-

crease in surface roughness is beneficial for the system to reduce the instability phenomenon. When the surface roughness exceeds a certain value, a smoother surface is more prone to unstable friction. Most noteworthy, the peak values of curves and instability boundary values are constant. Hence, it is difficult to improve the system stability within the range of 1.65 and 1.80 of the fractal dimension.

Similarly, the relationship between the speed and the real part of eigenvalues at four different loads is shown in Fig. 6. It can be seen from Fig. 6(b) that the instability trend of the system rises apparently with the increase in the applied load. Although the applied load has a great influence on system stability, its value should not be changed due to the index requirement in practical engineering. Fig. 7 depicts the variation of system stability trends under different Stribeck coefficients. Evidently, decreasing the Stribeck coefficient makes the system more unstable, but can reduce the system instability boundary value and expand the stability interval. Actually, it is an extremely complex procedure to vary the Stribeck coefficient affected by nonlinear factors. Hence, the selection of the Stribeck coefficient should be determined according to the particular system requirements.

By comparing Fig. 4 to Fig. 7, it can be concluded that the instability boundary value and the speed corresponding to the peak value are not changed with the parameters of D, G or p, while they are influenced by the Stribeck coefficient. No matter how the other parameters are changed with the determined value of the Stribeck coefficient, only the trend of the system instability is changeable. Moreover, a proper surface roughness can reduce the system instability, but the smoother the surface, the more likely it is to cause friction instability.

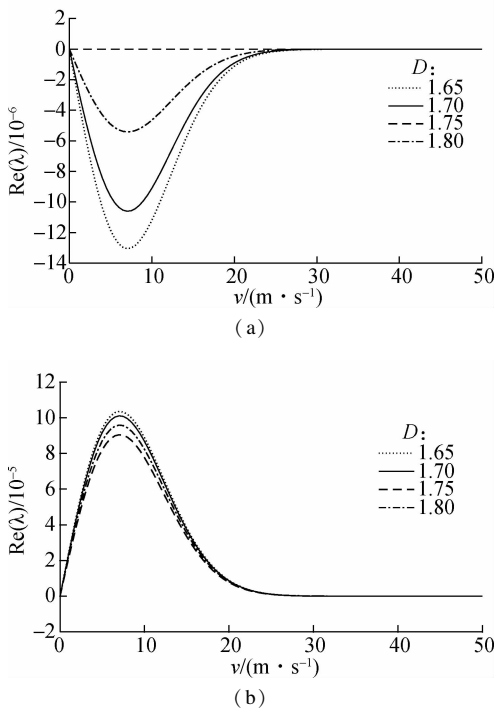

Fig. 4 Effects of the fractal dimension D on the real part of eigenvalues. (a) The second-order eigenvalue; (b) The third-order eigenvalue

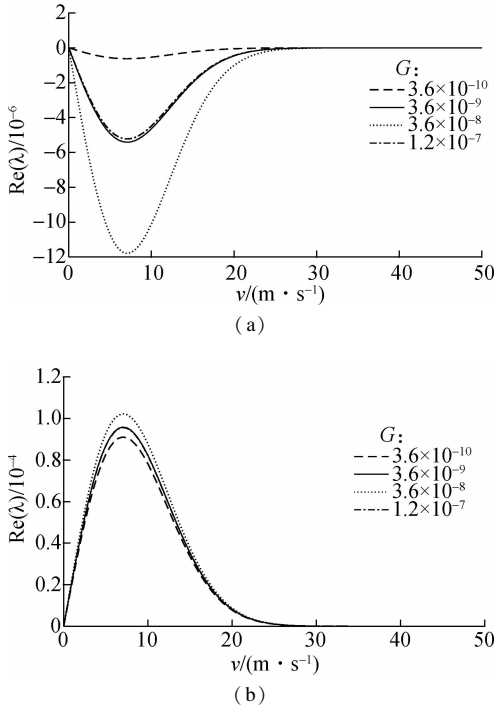

Fig. 5 Effects of the fractal scaling coefficient G on the real part of eigenvalues. (a) The second-order eigenvalue; (b) The third-order eigenvalue

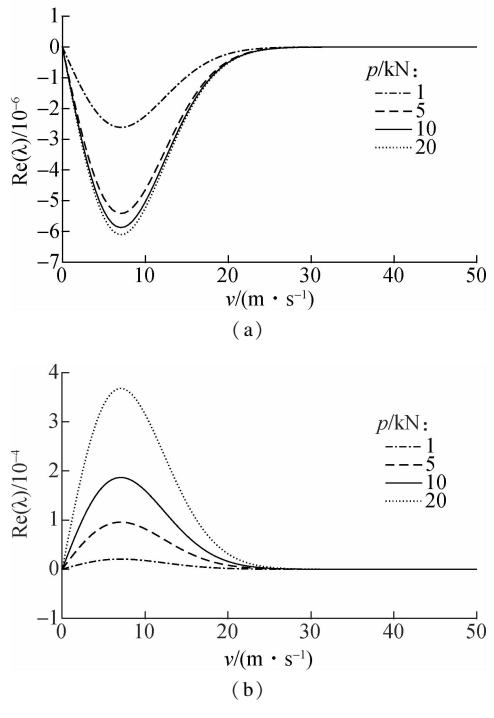

Fig. 6 Effects of the applied load p on the real part of eigenvalues. (a) The second-order eigenvalue; (b) The third-order eigenvalue

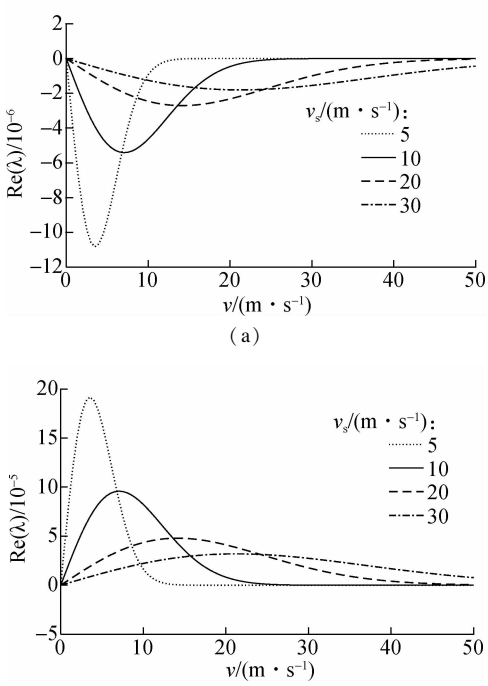

Fig. 7 Effects of the Stribeck coefficient v_s on the real part of eigenvalues. (a) The second-order eigenvalue; (b) The third-order eigenvalue

5 Conclusions

1) The rotating tribological pair system on the end face exhibits an unstable state at low speed and gradually enters a steady state at high speed.

2) The real part of the first-order eigenvalue of the system is always zero, and the third-order eigenvalue causes the system instability.

3) The fractal dimension and the fractal scaling coefficient have a slight impact on system stability when fractal dimensions are large, but there are optimal values for minimizing the instability trend of the system, which means that there is a best value for the surface roughness.

4) Reducing the applied load and Stribeck coefficient can improve system stability; and the instability boundary value is only altered by the Stribeck coefficient.

References

[1] Akay A. Acoustics of friction[J]. *The Journal of the Acoustical Society of America*, 2002, **111**(4): 1525 - 1548. DOI:10.1121/1.1456514.

[2] Suzuki H, Miura R. The jerking motion in servomechanisms, considering negative slope of friction characteristics[J]. *Transactions of the Institute of Electrical Engineers of Japan A*, 1967, **87**(Supp S1): 1321 - 1330.

[3] Spurr R T. A theory of brake squeal[J]. *Proceedings of the Institution of Mechanical Engineers: Automobile Division*, 1961, **15**(1): 33 - 52. DOI:10.1243/pime_auto_1961_000_009_02.

[4] Popp K, Stelter P. Stick-slip vibrations and chaos[J]. *Philosophical Transactions of the Royal Society of London Series A: Physical and Engineering Sciences*, 1990, **332**(1624): 89 - 105. DOI:10.1098/rsta.1990.0102.

[5] Hoffmann N, Gaul L. Effects of damping on mode-coupling instability in friction induced oscillations[J]. *ZAMM*, 2003, **83**(8): 524 - 534. DOI:10.1002/zamm.200310022.

[6] Crowther A R, Singh R. Analytical investigation of stick-slip motions in coupled brake-driveline systems[J]. *Nonlinear Dynamics*, 2007, **50**(3): 463 - 481. DOI:10.1007/s11071-006-9187-9.

[7] Giannini O, Massi F. Characterization of the high-frequency squeal on a laboratory brake setup[J]. *Journal of Sound and Vibration*, 2008, **310**(1/2): 394 - 408. DOI:10.1016/j.jsv.2007.08.009.

[8] Devarajan K, Balaram B. Analytical approximations for stick-slip amplitudes and frequency of duffing oscillator[J]. *Journal of Computational and Nonlinear Dynamics*, 2017, **12**(4): 044501. DOI:10.1115/1.4034734.

[9] Abdo J, Abouelsoud A A. Analytical approach to estimate amplitude of stick-slip oscillations[J]. *Journal of Theoretical and Applied Mechanics*, 2011, **49**(4): 971 - 986.

[10] Niknam A, Farhang K. Vibration instability in a large motion bistable compliant mechanism due to stribeck friction[J]. *Journal of Vibration and Acoustics*, 2018, **140**(6): 061017. DOI:10.1115/1.4040513.

[11] Xiang W, Yan S Z, Wu J N. Dynamic analysis of planar mechanical systems considering stick-slip and Stribeck effect in revolute clearance joints[J]. *Nonlinear Dynamics*, 2019, **95**(1): 321 - 341. DOI:10.1007/s11071-018-4566-6.

[12] Ouyang H, Mottershead J E, Cartmell M P, et al. Friction-induced vibration of an elastic slider on a vibrating disc[J]. *International Journal of Mechanical Sciences*, 1999, **41**(3): 325 - 336. DOI:10.1016/s0020-7403(98)00059-9.

[13] Ouyang H, Mottershead J E. Dynamic instability of an elastic disk under the action of a rotating friction couple[J]. *Journal of Applied Mechanics*, 2004, **71**(6): 753 - 758. DOI:10.1115/1.1795815.

[14] Kang J. Theoretical model for friction-induced vibration of ball joint system under mode-coupling instability[J]. *Tribology Transactions*, 2015, **58**(5): 807 - 814. DOI:10.1080/10402004.2015.1020121.

[15] Sui X, Ding Q. Instability and stochastic analyses of a pad-on-disc frictional system in moving interactions[J]. *Nonlinear Dynamics*, 2018, **93**(3): 1619 - 1634. DOI:10.1007/s11071-018-4280-4.

[16] Pohrt R, Popov V L. Normal contact stiffness of elastic solids with fractal rough surfaces[J]. *Physical Review Letters*, 2012, **108**(10): 104301. DOI:10.1103/physrevlett.108.104301.

[17] Guan D, Jing L, Hilton H H, et al. Tangential contact analysis of spherical pump based on fractal theory[J]. *Tribology International*, 2018, **119**: 531 - 538. DOI:10.1016/j.triboint.2017.11.034.

[18] Sun Y Y, Xiao H F, Xu J W, et al. Study on the normal contact stiffness of the fractal rough surface in mixed lubrication[J]. *Proceedings of the Institution of Mechanical Engineers, Part J: Journal of Engineering Tribology*,

2018, **232** (12): 1604 - 1617. DOI: 10.1177/1350650118758741.

[19] Xiao H F, Sun Y Y, Chen Z G. Fractal modeling of normal contact stiffness for rough surface contact considering the elastic-plastic deformation[J]. *Journal of the Brazilian Society of Mechanical Sciences and Engineering*, 2019, **41**: No. 11. DOI:10.1007/s40430-018-1513-x.

[20] Liu P, Zhao H, Huang K, et al. Research on normal contact stiffness of rough surface considering friction based on fractal theory[J]. *Applied Surface Science*, 2015, **349**: 43 - 48. DOI:10.1016/j.apsusc.2015.04.174.

[21] Pan W J, Li X P, Wang L L, et al. A normal contact stiffness fractal prediction model of dry-friction rough surface and experimental verification[J]. *European Journal of Mechanics-A*, 2017, **66**: 94 - 102. DOI:10.1016/j.euromechsol.2017.06.010.

[22] Awrejcewicz J, Olejnik P. Analysis of dynamic systems with various friction laws[J]. *Applied Mechanics Reviews*, 2005, **58**(6): 389 - 411. DOI: 10.1115/1.2048687.

[23] Armstrong-Hélouvry B, Soom A. Control of machines with friction[J]. *Journal of Tribology*, 1992, **114**(3): 637. DOI:10.1115/1.2920929.

[24] Majumdar A, Bhushan B. Fractal model of elastic-plastic contact between rough surfaces[J]. *Journal of Tribology*, 1991, **113**(1): 1 - 11. DOI:10.1115/1.2920588.

[25] Liu W J, Tang F S. Modeling a simplified regulatory system of blood glucose at molecular levels[J]. *Journal of Theoretical Biology*, 2008, **252**(4): 608 - 620. DOI: 10.1016/j.jtbi.2008.02.021.

[26] Guan Z Z, Ye M H, Yin X C, et al. Recognition of surface roughness based on fractal theory and the microscopic images[J]. *Applied Mechanics and Materials*, 2012, **241/242/243/244**: 3030 - 3033. DOI: 10.4028/www.scientific.net/amm.241-244.3030.

[27] Pan Y L, Wu L Q, Zhang Y D. Study of the relationship between fractal model parameters and roughness parameter r_a[J]. *Engineering Science*, 2004, **6**(5): 49 - 51. (in Chinese)

圆盘端面旋转摩擦副系统稳定性分析

陈 龙 张建润

(东南大学机械工程学院, 南京 211189)

摘要:为了研究旋转摩擦副系统的摩擦和接触稳定性,考虑因素变化对稳定性的影响,建立了基于拉格朗日方程的系统动力学分析模型. 基于分形理论建立表面接触刚度模型,采用 Stribeck 摩擦效应建立摩擦力矩-速度模型,利用 Lyapunov 间接法数值研究系统状态方程的特征根问题,并具体讨论了外载荷、分形维数、分形尺度系数和 Stribeck 系数等参数对系统稳定性的影响. 数值仿真结果表明:摩擦副系统在低速时容易引起系统不稳定,随着 Stribeck 系数减小,系统不稳定边界值减小;在分形维数较大的情况下,分形维数和分形尺度系数略微影响系统的稳定性,并且适当提高表面光滑度可以降低系统不稳定性;系统不稳定性随着施加的载荷和 Stribeck 系数的增加而明显增强. 研究成果可为分析摩擦副系统的动态性能提供参考和理论支持.

关键词:旋转摩擦副系统;接触刚度;Stribeck 效应;动力学模型;稳定性

中图分类号:TH113;TH117